AD-A163 206 ELECTROMAGNETIC INSTABILITY IN A QUADRUPOLE-FOCUS ACCELERATOR(U) MISSION RESEARCH CORP ALBUQUERQUE NM T P HUGHES ET AL. OCT 85 AMRC-R-323 N00014-84-C-0078 1/1

UNCLASSIFIED F/G 20/7 NL

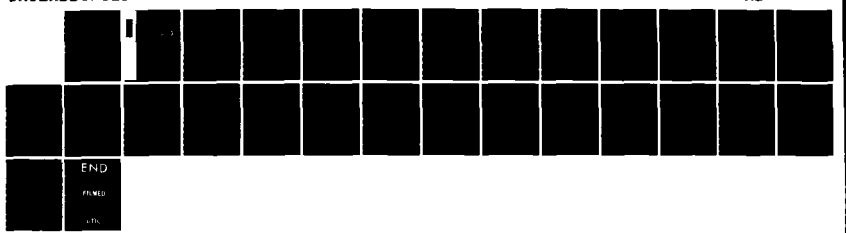

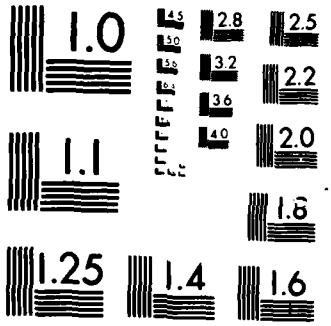

(12)

AMRC-N-323
Copy 23

ELECTROMAGNETIC INSTABILITY IN A QUADRUPOLE-FOCUSING ACCELERATOR

Thomas P. Hughes
Brendan B. Godfrey

October 1985

Prepared for: OFFICE OF NAVAL RESEARCH
Arlington, Virginia 22217

Under Contract: N00014-84-C-0078

Prepared by: MISSION RESEARCH CORPORATION
1720 Randolph Road, SE
Albuquerque, New Mexico 87106

UNCLASSIFIED

SECURITY CLASSIFICATION OF THIS PAGE (When Data Entered)

REPORT DOCUMENTATION PAGE	READ INSTRUCTIONS BEFORE COMPLETING FORM
1. REPORT NUMBER	2. GOVT ACCESSION NO. AD-A163206	3. RECIPIENT'S CATALOG NUMBER
4. TITLE (and Subtitle) ELECTROMAGNETIC INSTABILITY IN A QUADRUPOLE-FOCUSING ACCELERATOR	5. TYPE OF REPORT & PERIOD COVERED
	6. PERFORMING ORG. REPORT NUMBER AMRC-N-323
7. AUTHOR(s) Thomas P. Hughes, Brendan B. Godfrey	8. CONTRACT OR GRANT NUMBER(s) N00014-84-C-0078
9. PERFORMING ORGANIZATION NAME AND ADDRESS MISSION RESEARCH CORPORATION, 1720 Randolph Road, SE, Albuquerque, NM 87106	10. PROGRAM ELEMENT, PROJECT, TASK AREA & WORK UNIT NUMBERS
11. CONTROLLING OFFICE NAME AND ADDRESS OFFICE OF NAVAL RESEARCH, Arlington, Virginia 22217	12. REPORT DATE October 1985
	13. NUMBER OF PAGES 25
14. MONITORING AGENCY NAME & ADDRESS(if different from Controlling Office)	15. SECURITY CLASS. (of this report) Unclassified
	15a. DECLASSIFICATION DOWNGRADING SCHEDULE

16. DISTRIBUTION STATEMENT (of this Report)

Distribution in whole or in part is permitted for any purpose of the United States Government. Approved for public release: distribution unlimited.

17. DISTRIBUTION STATEMENT (of the abstract entered in Block 20, if different from Report)

18. SUPPLEMENTARY NOTES

19. KEY WORDS (Continue on reverse side if necessary and identify by block number)

High current betatrons
Quadrupole focusing
Three-wave interaction

20. ABSTRACT (Continue on reverse side if necessary and identify by block number)

The addition of helical focusing to a modified betatron configuration is shown to give rise to an electromagnetic instability under certain conditions. The instability arises from a three-wave coupling between the helical field, a transverse mode on the beam, and a transverse-electric waveguide mode. An analytic dispersion relation is derived. Several features of the instability are confirmed using three-dimensional computer simulations.

DD FORM 1 JAN 73 1473 EDITION OF 1 NOV 65 IS OBSOLETE

Unclassified

SECURITY CLASSIFICATION OF THIS PAGE (When Data Entered)

ABSTRACT

The addition of helical quadrupole focusing to a modified betatron configuration is shown to give rise to an electromagnetic instability under certain conditions. The instability arises from a three-wave coupling between the helical field, a transverse mode on the beam and a transverse-electric waveguide mode. An analytic dispersion relation is derived. Several features of the instability are confirmed using three-dimensional computer simulations.

CONTENTS

ILLUSTRATIONS

I. INTRODUCTION

Betatrons and other recirculating accelerator designs have been studied in recent years as compact accelerators for high-current electron beams.[1-6] Conventional[7] and modified[1] betatrons require precise matching of the beam energy to the vertical magnetic field if a fixed major radius is to be maintained. To overcome this restriction, strong focusing in the form of a helical magnetic quadrupole has been added to the modified betatron configuration.[3,8] This considerably increases the tolerance of the device to mismatch. In this paper, we show that helical quadrupole focusing can lead to an electromagnetic instability arising from a three-wave interaction between the static helical field, a transverse mode on the beam, and a transverse-electric (TE) waveguide mode. This behavior is reminiscent of that which occurs in planar geometry in the presence of a rippled magnetic field.[9] Unlike the free-electron laser instability, which was recently analyzed in the presence of helical quadrupole focusing,[10] longitudinal bunching of the beam plays no significant role in the instability which we describe here. Also, the instability is essentially independent of the radius of curvature of the device. It is thus not related to the negative-mass instability, for example. The main effect of finite radius of curvature is to discretize the toroidal mode-numbers. This can be important, since if the instability width is narrow enough, it can fall between two allowed mode-numbers and disappear (see Section II).

In Section II, we give an analytic theory of the instability. In Section III, we obtain a simplified dispersion relation which yields an instability criterion. Section IV details comparisons between the analytic theory and three-dimensional particle simulations. Section V gives our conclusions.

Throughout the paper, we use convenient units where the electron charge e and mass m, and the velocity of light c, are scaled out. Lengths are normalized to $c/\omega_0 \equiv 1$ cm, frequencies to ω_0, velocities to c, densities to $\omega_0^2 m/4\pi e^2$, electric and magnetic fields to $mc\omega_0/e$.

II. ANALYTIC MODEL OF INSTABILITY

The geometry and coordinate system we use are illustrated in Figure 1. An electron ring of major radius R and minor radius a circulates around the center of a conducting torus whose major and minor radii are R and b, respectively. The externally applied magnetic fields consist of a vertical field $B_z \propto r^{-s}$, where s is the external field index (we assume s = 1/2) a solenoidal field B_θ, and a helical quadrupole field B_q. This is the configuration of the stellatron accelerator.[3] A configuration where the helical quadrupole field is generated by two current-carrying wires instead of four also has been proposed.[6] We assume that the beam can be modeled as a string of rigid disks. This means that we follow the transverse motion of the beam centroid, and ignore any internal dynamics. This treatment is valid provided the drift-tube minor radius is much greater than the beam radius, $b \gg a$, since the fields we need to consider have a transverse scale length $\sim b$. We ignore the perturbed θ-motion of the beam under the assumption of relativisitic stiffness in this direction, i.e., $\gamma \gg 1$, where γ is the beam relativistic factor.

In equilibrium, the matched value of the vertical magnetic field is $B_z = \gamma V_\theta/R$, where V_θ is the toroidal beam velocity. Linearizing about the equilibrium position, we obtain the following equations of motion for the perturbed coordinates $\tilde{r}$, $\tilde{z}$ of the beam centroid.[3]

$$\ddot{\tilde{r}} + \frac{1}{2}\Omega_z^2\tilde{r} - \Omega_\theta\dot{\tilde{z}} + \mu\Omega_z^2(\tilde{r}\cos m\theta + \tilde{z}\sin m\theta) = -\tilde{E}_r - V_\theta\tilde{B}_z \quad , \tag{1}$$

$$\ddot{\tilde{z}} + \frac{1}{2}\Omega_z^2\tilde{z} + \Omega_\theta\dot{\tilde{r}} + \mu\Omega_z^2(\tilde{r}\sin m\theta - \tilde{z}\cos m\theta) = -\tilde{E}_z + V_\theta\tilde{B}_r \quad , \tag{2}$$

where a dot denotes the total time derivative $\partial/\partial t + (V_\theta/R)\partial/\partial\theta$, $\Omega_z = B_z/\gamma$, $\Omega_\theta = B_\theta/\gamma$, μ denotes the amplitude of the quadrupole field index, and $\tilde{E}$, $\tilde{B}$ denote the perturbed <u>self</u> electric and magnetic fields acting on

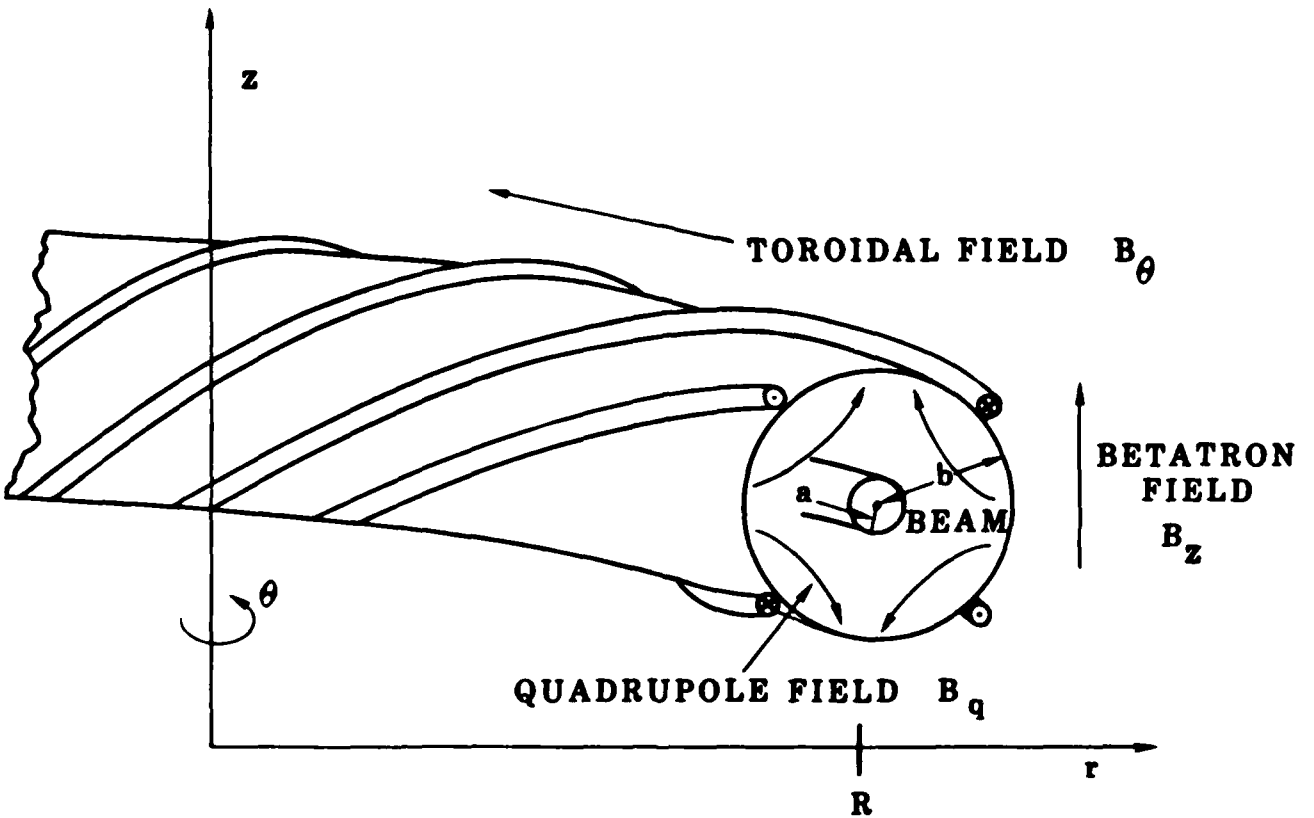

Figure 1. Geometry of stellatron accelerator showing conducting toroidal cavity and externally applied magnetic fields.

the beam at the perturbed position. Letting $\xi \equiv \tilde{z} + i\tilde{r}$, Eqs. (1), (2) can be written

$$\xi + \frac{1}{2}\Omega_z^2\xi - i\Omega_\theta\dot{\xi} - \mu\Omega_z^2 e^{-im\theta}\,\xi^* = -[\tilde{E}_z + i\tilde{E}_r + iV_\theta(\tilde{B}_z + i\tilde{B}_r)] \quad , \quad (3)$$

where * denotes the complex conjugate. To calculate $\underline{\tilde{E}}$, $\underline{\tilde{B}}$, we use a Green's function approach. Maxwell's equations can be written

$$\underline{\nabla} \times \underline{\nabla} \times \underline{E} - \omega^2\underline{E} = i\omega\underline{J} \quad , \quad (4)$$

$$\underline{B} = -\frac{i}{\omega}\underline{\nabla} \times \underline{E} \quad , \quad (5)$$

where we assume an $e^{-i\omega t + i\ell\theta}$ dependence for the perturbed fields and currents. The solution to Eq. (4) can be written down using a dyadic Green's function,[11] constructed from the solutions to the homogeneous counterpart of Eq. (4). The expressions obtained are infinite series.[12] The expression for $\tilde{E}_r$, for example, evaluated at the location of the beam, is

$$\tilde{E}_r = -\nu\omega(\omega - \ell\Omega_z)\tilde{r}\left[\sum_\eta \frac{I_\eta}{\eta^2 + \ell^2/R^2 - \omega^2}\right.$$

$$\left. - \sum_\lambda \frac{\ell^2/R^2\, I_\lambda}{(\lambda^2 + \ell^2/R^2 - \omega^2)(\lambda^2 + \ell^2/R^2)}\right] + O\left(\frac{b}{R}\right) + \frac{\partial E_r^0}{\partial r}\tilde{r} \quad , \quad (6)$$

where

$$I_\eta^{-1} = \frac{1}{2}\left[b^2 - \frac{1}{\eta^2}\right] J_1^2(\eta b) \quad , \quad I_\lambda^{-1} = \frac{b^2}{2}\,[J_1'(\lambda b)]^2 \quad ,$$

where J_1 is a Bessel function, and where η denotes the roots of $J_1'(\eta b) = 0$, λ denotes the roots of $J_1(\lambda b) = 0$, and $O(b/R)$ denotes toroidal corrections, which we neglect under the assumption $R \gg b$. Also, ν is Budker's parameter, i.e., the number of electrons per unit length of the beam times the classical electron radius. The last term in Eq. (6) results from evaluating the equilibrium radial electric field E_r^0 at the perturbed position.

In deriving Eq. (6), we have used the rigid-disk approximation to write $\tilde{J}_r = -\rho\dot{\tilde{r}} = i(\omega - \ell\Omega_z)\rho\tilde{r}$, where ρ is the beam density. Similar expressions are obtained for the other fields. To simplify the analysis, we extract from the series those terms containing the lowest root of $J_1'(\eta b) = 0$, denoted by η_{11}. These terms contain the transverse-electric TE_{11} resonance, which is the lowest electromagnetic waveguide resonance. All other self-field contributions are neglected. This procedure is equivalent to treating the beam as a weak perturbation of the vacuum TE_{11} eigenmode.

We now proceed to solve Eq. (3) by writing ξ in the form

$$\xi = \sum_{\ell} \xi_{\ell}^{+} e^{i\ell\theta - i\omega t} + \xi_{\ell}^{-} e^{i\ell\vartheta + i\omega t} \tag{7}$$

where +, - refer to "forward" and "backward" waves respectively. Substituting this into Eq. (3), we obtain the coupled equations

$$\left[-\Omega_+^2 + \frac{1}{2}\Omega_z^2 - \Omega_+\Omega_\theta + \frac{\alpha\Omega_+^2}{\omega^2 - \eta_{11}^2 - \ell^2/R^2} \right] \xi_{\ell}^{+} - \mu\Omega_z^2 (\xi_{-m-\ell}^{-})^* = 0 \quad , \tag{8a}$$

$$\left[-(\Omega_+ - m\Omega_z)^2 + \frac{1}{2}\Omega_z^2 + (\Omega_+ - m\Omega_z)\Omega_\theta + \frac{\alpha(\Omega_+ - m\Omega_z)^2}{\omega^2 - \eta_{11}^2 - (\ell + m)^2/R^2} \right] \xi_{-m-\ell}^{-} - \mu\Omega_z^2 (\xi_{\ell}^{+})^* = 0 \quad , \tag{8b}$$

$$\left[-\Omega_-^2 + \frac{1}{2}\Omega_z^2 + \Omega_-\Omega_\theta + \frac{\alpha\Omega_-^2}{\omega^2 - \eta_{11}^2 - \ell^2/R^2} \right] \xi_{\ell}^{-} - \mu\Omega_z^2 (\xi_{-m-\ell}^{+})^* = 0 \quad , \tag{8c}$$

$$\left[-(\Omega_- + m\Omega_z)^2 + \frac{1}{2}\Omega_z^2 - (\Omega_- + m\Omega_z)\Omega_\theta + \frac{\alpha(\Omega_- + m\Omega_z)^2}{\omega^2 - \eta_{11}^2 - (\ell + m)^2/R^2} \right] \xi_{-m-\ell}^{+} - \mu\Omega_z^2 (\xi_{\ell}^{-})^* = 0 \quad , \tag{8d}$$

where $\Omega_{\pm} = \omega \mp \ell\Omega_z$, $\alpha = \nu I_\eta/\gamma$ for $\eta = \eta_{11}$ ($\alpha \approx 8.4\nu/\gamma b^2$). Note that this is a closed system of equations, in which only mode-numbers ℓ and $-m - \ell$ appear. This is a consequence of the complex-conjugate sign appearing in Eq. (3). Further, note that ξ^+_ℓ is coupled only to $\xi^-_{-m-\ell}$, and ξ^-_ℓ is coupled only to $\xi^+_{-m-\ell}$. Thus the 4×4 matrix of Eq. (8) splits into two 2×2 matrices. The determinant of one 2×2 matrix gives the dispersion relation

$$\left[\Omega_+^2 - \frac{1}{2}\Omega_z^2 + \Omega\Omega_\theta - \frac{\alpha\Omega_+^2}{\omega^2 - \eta_{11}^2 - \ell^2/R^2}\right]\left[(\Omega_+ - m\Omega_z)^2\right.$$

$$\left. - \frac{1}{2}\Omega_z^2 - (\Omega_+ - m\Omega_z)\Omega_\theta - \frac{\alpha(\Omega_+ - m\Omega_z)^2}{\omega^2 - \eta_{11}^2 - (\ell + m)^2/R^2}\right] - \mu^2\Omega_z^4 = 0 \quad . \quad (9)$$

The determinant of the other 2×2 matrix can be obtained from Eq. (9) by letting $\omega \to -\omega$. Having obtained a root for ω from Eq. (9), the corresponding normal mode for ξ can be obtained from Eqs. (8a, 8b), and is a linear combination of two terms with space-time dependences $\exp(i\ell\theta - i\omega t)$ and $\exp[-i(m + \ell)\theta + i\omega t]$ respectively.

Multiplying out the dispersion relation in Eq. (9), we obtain an eighth degree polynomial in ω. Numerical solution for the sample parameters in Table I gives the set of curves shown in Fig. 2. The parameter ε in Table I is related to μ by $\mu = \varepsilon m\Omega_\theta/2\Omega_z$. The curves can be classified as follows:

$$\text{Electromagnetic modes:} \quad \omega^2 \approx \eta_{11}^2 + \ell^2/R^2 \ , \ \eta_{11}^2 + (m + \ell)^2/R^2 \ ,$$

$$\text{Cyclotron modes:} \quad \omega \approx (m + \ell)\Omega_z + \Omega_\theta \ , \ \ell\Omega_z - \Omega_\theta \ ,$$

$$\text{Low frequency transverse modes:} \quad \omega \approx (m + \ell)\Omega_z - \omega_B \ , \ \ell\Omega_z + \omega_B \ , \quad (10)$$

where $\omega_B \approx 1/4\ \Omega_z^2/\Omega_\theta$. These approximate forms are based on the assumption $\Omega_\theta \gg \Omega_z$, which is satisfied for typical stellatron parameters.

TABLE I. HIGH-CURRENT STELLATRON PARAMETERS USED IN PARTICLE SIMULATIONS

Torus Major Radius	1 m
Torus Minor Radius	8.4 - 9.5 cm
Beam Major Radius	1 m
Beam Minor Radius	2 cm
Beam Current (I)	300 A - 10 kA
Beam Energy (γ)	7
Toroidal Magnetic Field	5 kG
Vertical Magnetic Field	118 G
Quadrupole Field (ε)	0.7
Quadrupole Mode-Number	14-30

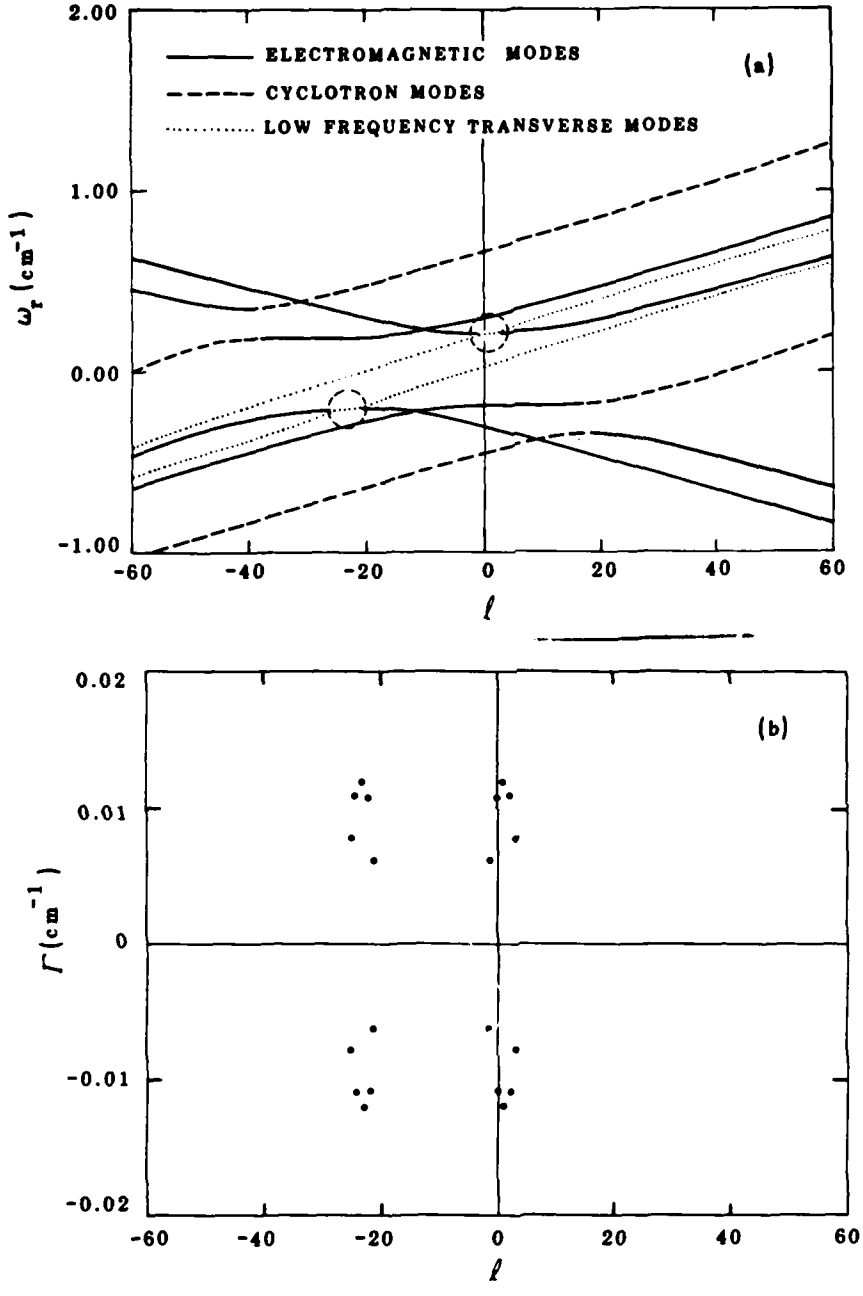

Figure 2. Frequencies and growth rates, denoted by ω_r and Γ, respectively, obtained from the dispersion relation Eq. (9), for Table I parameters with b = 8.8, I = 10 kA m = 22. In (a), the two unstable interactions are circled. In (b), growth rates at integer (allowed) values of ℓ are shown.

It can be shown from Eq. (9), and is apparent from Figure 2, that the dispersion relation is symmetrical about the line $\ell = -m/2$ (m is an even integer, equal to twice the number of minor turns the helical conductors make in going one major turn around the torus). More precisely, if we define $\ell' = \ell + m/2$, then $\omega \to -\omega^*$ as $\ell' \to -\ell'$. In the following, we will look only at $\ell' > 0$. Results for $\ell' < 0$ follow by symmetry.

Instability occurs due to the intersection of the curve $\omega \approx (m + \ell)\Omega_z - \omega_B$ with the electromagnetic mode $\omega \approx \sqrt{n_{11}^2 + \ell^2/R^2}$. The instability can be thought of as a parametric process[13] in which the quadrupole field plays the role of a pump wave. If we denote the three interacting modes by subscripts 1,2,3, then we get the following frequencies and mode-numbers:

$$\text{Pump wave:} \quad \omega_1 = 0 \ , \ k_1 = m/R \ ,$$

$$\text{Electromagnetic wave:} \quad \omega_2 = \sqrt{n_{11}^2 + \ell^2/R^2} \ , \ k_2 = \ell/R \ ,$$

$$\text{Slow transverse wave:} \quad \omega_3 \approx (m + \ell)\Omega_z \ , \ k_3 = (m + \ell)/R \ , \qquad (11)$$

In terms of this picture, instability occurs when the usual matching conditions are approximately satisfied ($\omega_1 + \omega_2 = \omega_3$, $k_1 + k_2 = k_3$). Energy for the instability is provided by the beam via the negative-energy slow transverse mode.

III. DERIVATION OF INSTABILITY CRITERION

An approximate expression for the growth rate can be obtained by letting $\omega = \omega_{11} + \delta$, where $\omega_{11} = (\eta_{11}^2 + \ell^2/R^2)^{1/2}$ in Eq. (9), and keeping terms to order δ^2. This gives the quadratic expression

$$
\begin{aligned}
&-2\omega_{11}(\omega_{11} - \ell\Omega_z)(\omega_{11} - \ell\Omega_z + \Omega_\theta)\Omega_\theta\delta^2 \\
&\quad + \Big\{2\omega_{11}(\omega_{11} - \ell\Omega_z)(\omega_{11} - \ell\Omega_z + \Omega_\theta)[(\ell + m)\Omega_z - \omega_{11}]\Omega_\theta \\
&\quad + (\omega_{11} - \ell\Omega_z)^2\,\alpha\Omega_\theta - 2\omega_{11}\mu^2\Omega_z^4\Big\}\delta - \alpha(\omega_{11} - \ell\Omega_z)^2 \\
&\quad \times [(m + \ell)\Omega_z - \omega_{11}]\Omega_\theta = 0 \quad . \qquad (12)
\end{aligned}
$$

Defining the quantities γ_1, γ_2, γ_3 by

$$
\begin{aligned}
\gamma_1 &= 2\omega_{11}(\omega_{11} - \ell\Omega_z)(\omega_{11} - \ell\Omega_z + \Omega_\theta)[(\ell + m)\Omega_z - \omega_{11}]\Omega_\theta \quad , \\
\gamma_2 &= \alpha(\omega_{11} - \ell\Omega_z)^2\Omega_\theta \quad , \qquad (13) \\
\gamma_3 &= 2\omega_{11}\,\mu^2\Omega_z^4 \quad ,
\end{aligned}
$$

the condition for instability can be written

$$(\gamma_1 + \gamma_2 - \gamma_3)^2 < 4\gamma_1\gamma_2 \quad , \qquad (14a)$$

or, equivalently,

$$(\gamma_1 - \gamma_2 - \gamma_3)^2 < 4\gamma_2\gamma_3 \quad , \qquad (14b)$$

Equations (12)-(14) allow us to make some more exact statements about the conditions for instability. From Eqs. (13) and (14b), we see that the instability disappears for $\mu = 0$, as one would expect. Equation (14a) shows that $(\ell + m)\Omega_z > \omega_{11}$ (i.e. $\gamma_1 > 0$) is required for instability (assuming $\Omega_\theta > 0$; the case $\Omega_\theta < 0$ is discussed later). This means that the instability turns on when the frequency of the transverse beam mode is somewhat above the TE_{11} eigenfrequency, rather than exactly equal to it.

To see how the instability turns off as ℓ increases, we rewrite Eq. (14a) to obtain

$$\mu^2 > \frac{\left(\sqrt{\gamma_1} - \sqrt{\gamma_2}\right)^2}{2\omega_{11}\,\Omega_z^4} \quad , \tag{15}$$

as the criterion for instability. The term γ_1 is sensitive to the value of ℓ through the factor $(\ell + m)\Omega_z - \omega_{11}$. As ℓ increases, γ_1 eventually becomes large enough to violate this inequality, and the instability disappears (cf. Figure 2). Equation (15) also shows that as $\nu \to 0$, (so that $\gamma_2 \to 0$), and $\mu \to 0$, the unstable region in ℓ-space becomes narrower. If ℓ were a continuous variable, then the instability would persist near $(\ell + m)\Omega_z = \omega_{11}$ as long as ν and μ were finite. Since ℓ is discrete in a toroidal system, however, the unstable region can fall between two integer values of ℓ, and no instability would be seen.

Finally, from Eqs. (12) and (14a), the peak growth rate as a function of μ is found when μ is chosen so that $\gamma_1 + \gamma_2 - \gamma_3 = 0$. The growth rate Γ is then given by

$$\Gamma^2 = \frac{\alpha}{2} \frac{[(m + \ell)\Omega_z - \omega_{11}](\omega_{11} - \ell\Omega_z)}{\omega_{11}(\omega_{11} - \ell\Omega_z + \Omega_\theta)} \quad . \tag{16}$$

For the parameters of Fig. 2, this equation predicts $\Gamma = 1.06 \times 10^{-2}$ for $\ell = 0$, in good agreement with the exact result of 1.12×10^{-2} which occurs for $\varepsilon = 0.8$ ($\mu \approx 380$).

Thus far, we have assumed $\Omega_\theta > 0$. If Ω_θ is negative, then Eq. (14b) shows that the instability disappears. This is to be expected since the slow transverse wave then becomes a fast, positive energy wave. At the same time, the cyclotron wave $\omega \approx (m + \ell)\Omega_z + \Omega_\theta$ becomes a slow wave, with the potential for an unstable interaction. We have not examined this case, however, since previous calculations[3] have shown that the parameter space in which single particle orbits are stable shrinks greatly when the sign of Ω_θ is opposite to that of m.

IV. COMPARISON WITH NUMERICAL SIMULATIONS

To verify the above analytic calculations, we have performed three-dimensional numerical particle simulations with the code IVORY. For these simulations, field quantities are assumed to have the form

$$F(r,\theta,z,t) = \sum_n f_n(r,z,t)\, e^{in\theta} \quad . \tag{17}$$

In the r-z plane, field quantities are represented on a two-dimensional spatial mesh. The self-consistent fields of the beam are advanced in time using the full Maxwell's equations. Particles are advanced using the full Lorentz force equations. The stellatron fields are computed from analytic expressions.[3] In deciding on parameters for the simulations, computing costs constrain us to choose cases which minimize the running time and storage requirements. Thus, we concentrate on cases with large expected growth rates. In addition, we choose either $\ell = 0$, or choose $m + \ell$ to be a small integer multiple of ℓ. This minimizes the number of particles needed to resolve the different mode-numbers. For $\ell = 0$, for example, we see from Eqs. (11) and (17) that only mode-numbers 0, $\pm m$, must be represented in the simulations.

Choosing $\ell = 0$, we used the parameters in Table I with b = 8.8 cm and a 10 kA beam current, and performed simulations for different values of the quadrupole mode-number m. The growth-rates obtained are plotted in Fig. 3 versus those obtained from Eq. (9). We also show the growth rate from a simulation for m = 22 in which the beam was represented by a string of rigid disks in the code, instead of the more realistic particle representation. There are at least two possible reasons why agreement with the analytic result is better for the rigid disk simulation. First, the initial field energy level is lower for the latter due to the absence of internal degrees of freedom of the beam, so that there is a longer visible period of linear growth. In the simulations with particles, the field energy only increases only about one order of magnitude over its initial value before saturating, as shown in Figure 4. This means that the growth measured may not be truly exponential. Second, in the particle simulations

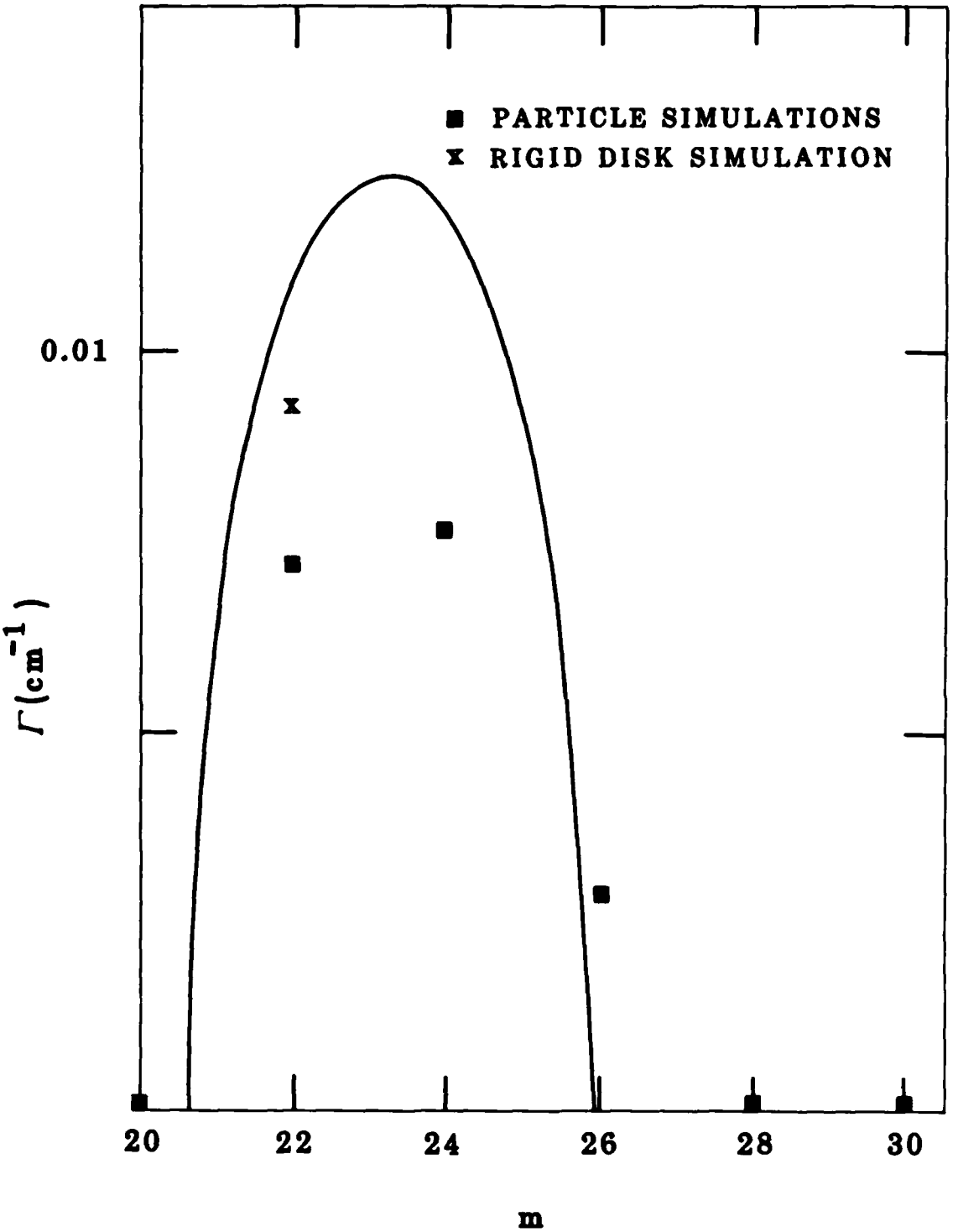

Figure 3. Growth rates of instability versus quadrupole mode-number m (which must be an even integer) for parameters in Table I, and b = 8.8 cm, I = 10 kA. Theoretical results (solid line) are compared to simulation-code results.

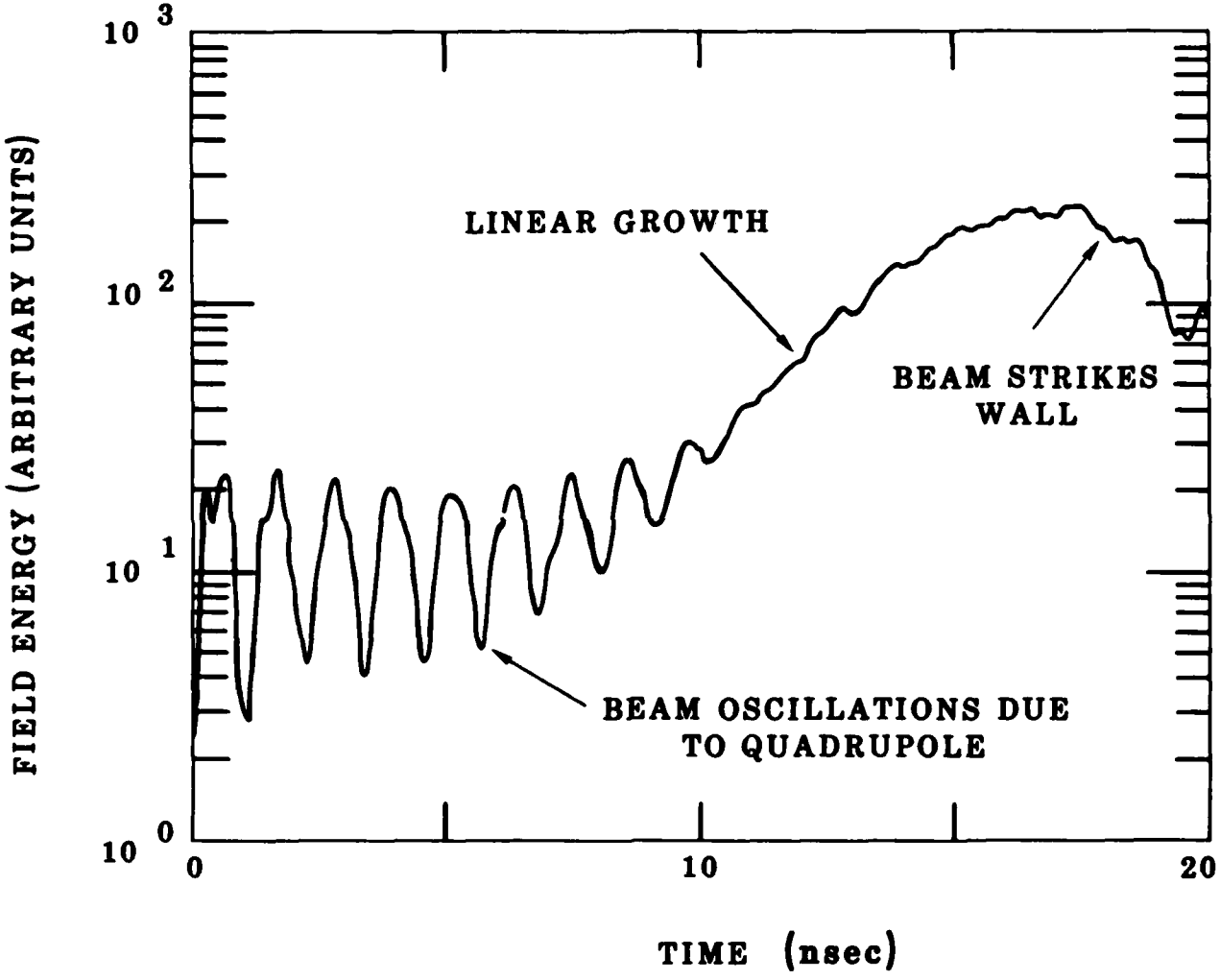

Figure 4. Energy in n = 22 field components (n = toroidal mode-number) versus time showing development of $\ell = 0$, m = 22 instability in Figure 2. This plot was generated by the simulation-code IVORY.

there is a spread in the energy of the particles due to space-charge, giving rise to a spread in transverse oscillation frequencies. This may have a stabilizing effect.

There is good agreement between simulations and theory as to the turn-on and turn-off of the instability. The TE_{11} cutoff frequency for the drift-tube is $\eta_{11} \approx 1.84/b \approx 0.21$. Figure 3 shows that, in agreement with the analytic prediction (Sec. III) instability sets in for $m > \eta_{11}/\Omega_z \approx 21$. No instability is seen during the length of the simulations for $m \geq 28$ (we ran cases for m = 28, 30).

Further evidence of the electromagnetic character of the instability comes from two simulations where the minor cross-section of the drift-tube was varied keeping m fixed. For m = 20, I = 10 kA, b = 8.8 cm (other parameters as in Table I), no growth was observed, since $m/R < 1.84/b$. On increasing the minor radius to 9.5 cm, however, strong growth was observed. In addition, a field contour plot of the n = 0 component of the perturbed B_θ, shown in Figure 5, reveals a TE_{11} structure.

In order to see whether the aspect ratio of the torus affects the instability, we increased the major radius R first to 10 m and then to 100 m, keeping m/R fixed at 0.22 and choosing $\ell = 0$. No significant change in the growth-rate was observed in the simulations. This is in contrast to the negative-mass instability,[14] where the growth rate typically falls off as 1/R.

Next, we tested the $\nu^{1/2}$ dependence of the growth rate on the beam current predicted by Eq. (16). The parameters in Table I with b = 9.0 cm, m = 22 were used to perform simulations at 300 A, 1 kA and 10 kA beam currents.The results in Figure 6 show that the predicted scaling is supported by the simulations.

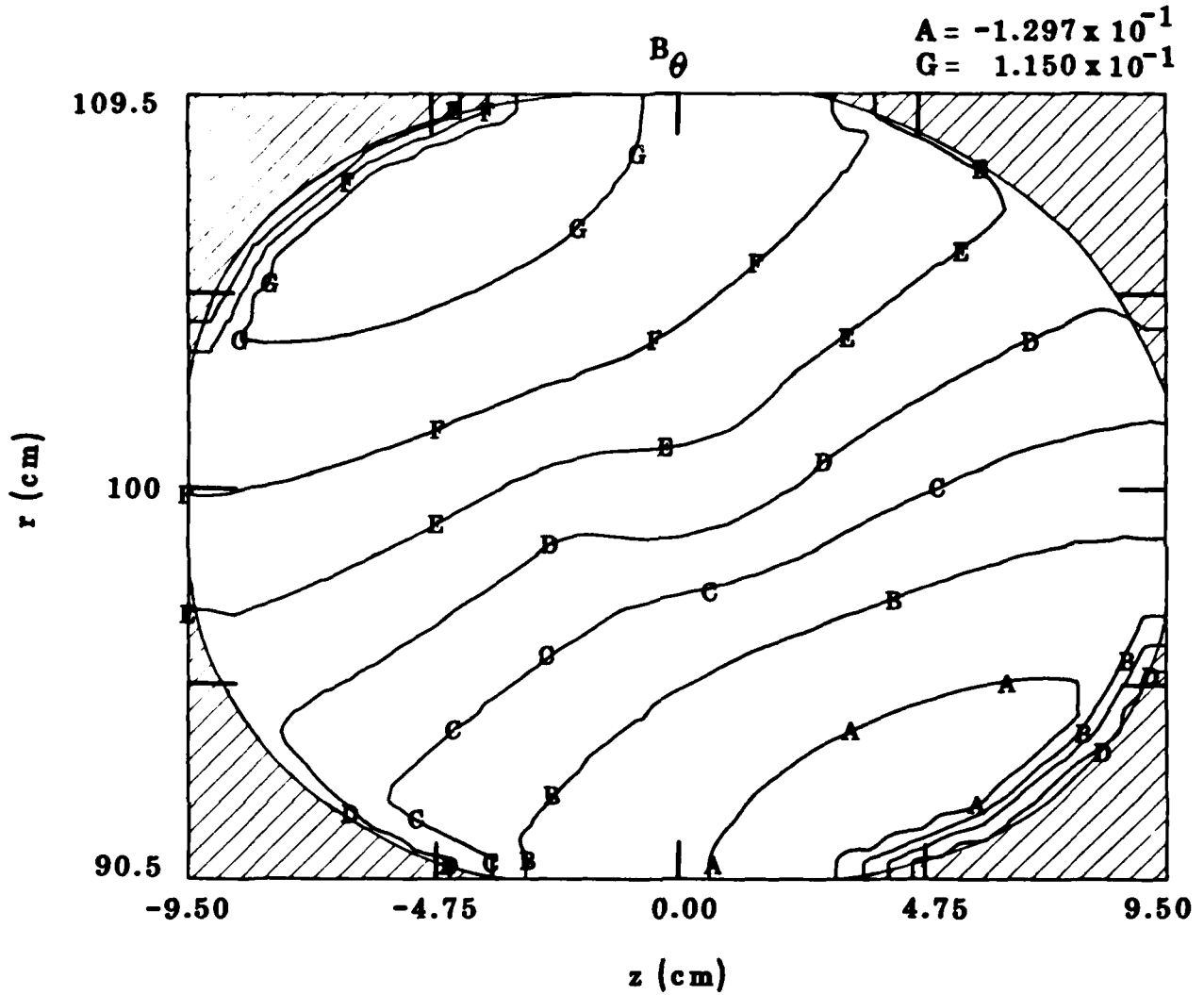

Figure 5. Contour plot of n = 0 component of toroidal self-magnetic field B_- during early nonlinear growth of and ℓ = 0, m = 20 instability. The contours have linearly increasing values from A to G. The structure is that of a TE_{11} mode. The distortion of contours in the center is due to the presence of the beam.

Thus far, we have reported on results for $\ell = 0$. Now, we look at a case for which $\ell = m = 14$. The dispersion diagram for this case, obtained from Eq. (9), is similar to that in Figure 2, except that one of the unstable regions occurs around $\ell = 14$. The simulation parameters used are those in Table I, with I = 10 kA, b = 8.4 cm chosen to enhance the growth rate. From Eqs. (11), (17), we see that mode-numbers 0, $\pm\ell$, $\pm(\ell + m)$ must be represented in the simulation code ($\ell = 0$ must always be present to represent the equilibrium fields). Field energy in the modes $|n| = \ell$, $(\ell + m)$ is observed to grow exponentially at a rate $\Gamma = 6.3 \times 10^{-3}$, compared to the analytic rate 7.8×10^{-3}. In this case it is the $|n| = 14$ field plots which show a TE mode character similar to that in Figure 4.

The nonlinear development of the instability is an important issue. To address it completely, many modes would have to be kept in the simulation code, since nonlinear effects give rise to the generation of modes other than those involved in the linear growth stage. However, we believe that the simulation results with just the linear modes present may give a good guide to the nonlinear development of the instability for the following reasons. First, the quadrupole field gives a initial perturbation to the mode number m, so that the fields in this mode are not growing from random noise (see Figure 4). Second, although wave-wave interactions are not treated correctly if we do not include other modes, the wave-particle interactions are treated nonlinearly. The simulations show that in those cases with large linear growth rates, which we can therefore afford to run to "saturation", the wave amplitude grows until the beam strikes the wall (see Figure 4). As a result, most of the beam particles are lost, leaving a large amplitude TE_{11} wave in the drift-tube.

Finally, we look at what our analysis predicts for the stellatron experiment presently under way at the University of California at Irvine (UCI).[15,16] The parameters for this experiment are tabulated in Table II. Because of the low current, the width of the instability is quite narrow, extending over at most one ℓ-number. As a result, small changes in

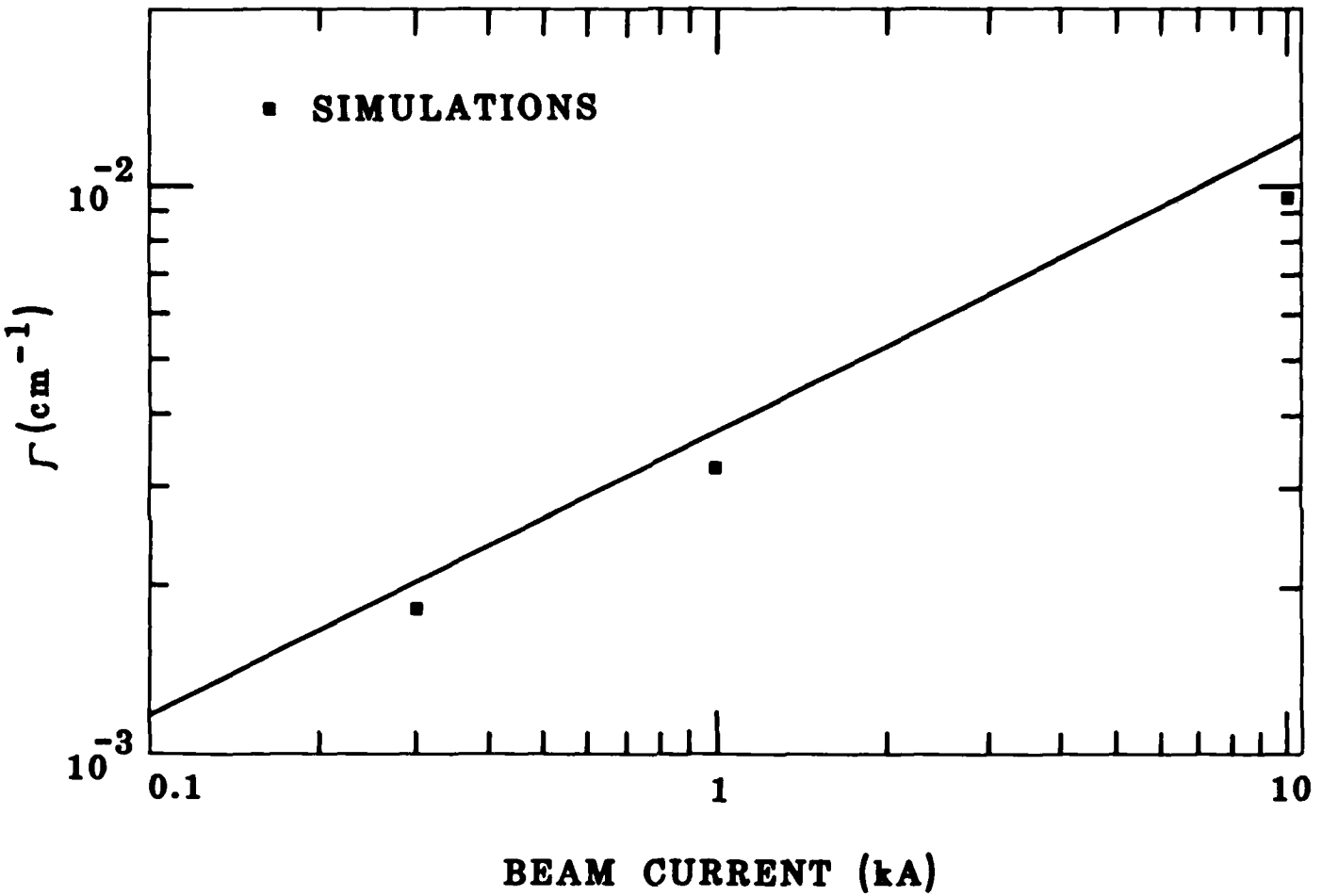

Figure 6. Growth rate of instability versus beam current for Table I parameters with m = 22, b = 9.0. Simulation results are compared to theoretical prediction.

parameters can cause the instability to abruptly appear and disappear [cf. Section III]. We find that the beam is unstable in the region $\gamma = 2.4$ to 2.45. With a one-turn accelerating voltage[15] of 500 V, the beam would spend sufficient time in this region to undergo 5-6 e-foldings. This instability may be related to the current disruption seen on some shots during the early part of the acceleration.[16] We emphasize that this is a tentative explanation. It has also been suggested that the negative-mass instability may be responsible for this disruption.[16]

TABLE II. PARAMETERS OF UCI STELLATRON

Torus Major Radius	41 cm
Torus Minor Radius	4 cm
Beam Current	200 A
Beam Energy	20 kV - 4 MeV
Toroidal Magnetic Field	0 - 10 kG
Vertical Magnetic Field	0 - 400 G
Quadrupole Field (ε)	0.18
Quadrupole Mode-Number	12

V. SUMMARY AND CONCLUSIONS

We have derived a dispersion relation for a parametric electromagnetic instability in a stellatron accelerator. The instability arises from the interaction between the quadrupole winding, a negative-energy transverse wave on the beam, and an electromagnetic wave-guide mode. The growth rate of the instability is independent of the radius of the toroidal drift-tube. It therefore occurs in straight as well as toroidal systems. Three-dimensional numerical simulations of the stellatron have been carried out with the code IVORY. The simulated linear growth rates and conditions for the onset of the instability are in reasonably good agreement with the analytic model. The simulations show strong disruption of the beam in the nonlinear regime, leading to loss of current. Our calculations predict some growth of the instability for the parameters of the UCI stellatron experiment. The instability may be a factor in limiting the beam current in this experiment.

VI. ACKNOWLEDGMENTS

We thank Dr. D. Chernin for useful discussions. This work was funded by the Office of Naval Research.

REFERENCES

1. P. Sprangle, C. A. Kapetanakos, and S. J. Marsh, Proc. IVth Intl. Conf. on High Power Electron and Ion Beams (Palaiseau, France, 1981).

2. C. W. Roberson, IEEE Nuc. Sci. NS-28, 3433 (1981).

3. C. W. Roberson, A. Mondelli, and D. Chernin, Phys. Rev. Lett. 50, 507 (1983).

4. D. P. Taggart, M. R. Parker, H. J. Hopman, R. Jayakumar, and H. H. Fleischmann, Phys. Rev. Lett. 52, 1601 (1984).

5. H. Ishizuka, G. Lindley, B. Mandelbaum, A. Fisher, and N. Rostoker, Phys. Rev. Lett. 53, 266 (1984).

6. C. Agritellis, C. A. Kapetanakos, S. J. Marsh, A. Prakash, and P. Sprangle, Bull. Am. Phys. Soc. 29, 1430 (1984).

7. D. W. Kerst, Phys. Rev. 58, 841 (1940).

8. B. Mandelbaum, H. Ishizuka, A. Fisher, and N. Rostoker, Bull. Am. Phys. Soc. 29, 1431 (1984).

9. W. M. Manheimer and E. Ott, Phys. Fluids 17, 463 (1974).

10. B. Levush, T. M. Antonsen, W. M. Manheimer, and P. Sprangle, Phys. Fluids 28, 2273, (1985).

11. C. T. Tai, Dyadic Green's Functions in Electromagnetic Theory (Intex: Educational Publishers, Scranton, 1971). Later work has shown that the Green's function representation in this book is incomplete [e.g. W. A. Johnson, A. Q. Howard and D. G. Dudley, Radio Science 14, 961 (1979)]. However, the missing terms do not contain electromagnetic resonances and so do not change our result.

12. T. P. Hughes and B. B. Godfrey, AMRC-R-655, Mission Research Corporation, Albuquerque (1984). [Defense Technology Information Center No. A151420].

13. V. P. Silin, Zh. Eksp. Teor. Fiz. 48 1679 (1965) [Sov. Phys-JETP 21, 1127 (1965)].

14. B. B. Godfrey and T. P. Hughes, Phys. Fluids 28, 669 (1985).

15. H. Ishizuka, G. Leslie, B. Mandelbaum, A. Fisher, and N. Rostoker, Bull. Am. Phys. Soc. 30, 983 (1985) [presented at 1985 Particle Accelerator Conference, Vancouver].

16. B. Mandelbaum, Ph. D. Thesis Dissertation, University of California at Irvine (1985).

END

FILMED

3-86

DTIC